Chemical Engineering Journal 480 (2024) 148330

Contents lists available at ScienceDirect

Chemical Engineering Journal

journal homepage: www.elsevier.com/locate/cej

Highly active Co_1-N_3-O_1 single-atom catalyst for boosting catalytic synthesis of unsaturated benzylamines and arylamines

Song Han [1], Ming-Shuai Sun [1], Wen-Ting Chen, Yan Zhou, Duan-Jian Tao [*]

National Engineering Research Center for Carbohydrate Synthesis, Key Laboratory of Fluorine and Silicon for Energy Materials and Chemistry of Ministry of Education, College of Chemistry and Chemical Engineering, Jiangxi Normal University, Nanchang 330022, China

ARTICLE INFO

Keywords:
Single-atom catalyst
Cobalt
Asymmetric coordination
Unsaturated amines
Reduction amination

ABSTRACT

Unsaturated benzylamines and arylamines are the key building blocks for the synthesis of organic pharmaceutical molecules, but their synthetic processes always suffer from low selectivity as a result of the excessive hydrogenation of unsaturated groups. Herein, the cobalt single-atom catalyst with an asymmetric Co_1-N_3-O_1 structure was designed and constructed on porous carbon nanospheres. It is found that the Co_1-N_3-O_1 catalyst showed excellent catalytic activity toward the synthesis of unsaturated benzylamines and arylamines. The results of characterization analysis and density functional theory (DFT) calculation further clarify that introducing oxygen into the Co single-atom coordination environment of Co_1-N_3-O_1 increased hydrogenation energy barrier of the terminal C=C double bond, which is beneficial to suppress competing hydrogenation reactions. Meanwhile, the Co_1-N_3-O_1 catalyst had the lower energy barrier for reduction of the C=N bond to amino group, boosting the yields of unsaturated benzylamines and arylamines. This study offers an attracting strategy for efficient and selective reductive amination reaction by making use of the asymmetrically structured Co single-atom catalyst.

1. Introduction

Benzylamines bearing unsaturated groups are important chemical intermediates in the field of pharmaceutical, fine chemical and plastics industries [1–5]. As shown in Fig. 1, 4-vinylbenzylamine is the key raw material for the synthesis of the lipid-lowering drug Cholestyramine and strongly basic polystyrene anion-exchange resin [6]. Also, the targeted therapy drug Erlotinib can treat non-small cell lung cancer and efficiently prolongs survival time, which is synthesized using the raw material 3-ethynylaniline. However, compared with the ammonolysis of 4-vinylbenzyl chloride to 4-vinylbenzylamine, the selective reductive amination of 4-vinylbenzaldehyde is a very attractive route but remains a big challenge. The common Rainey Ni and Pd/C heterogeneous catalysts are very easy to hydrogenate the vinyl and acetenyl groups, resulting in poor selectivity of unsaturated benzylamines and arylamines [7,8].

Recently, single-atom catalysts have exhibited great value in the field of heterogeneous catalysis owing to their high atomic utilization and adjustable coordination structure [9–14]. Furthermore, single-atom catalysts demonstrate excellent catalytic activity in many reduction reactions, such as aldehyde reduction [15,16], alkyne semi-hydrogenation [17], nitro-reduction [18–20] and CO_2 reduction reaction [21,22]. For example, Wang et al. reported that Co_1-N_4 single-atom on the α-cellulose derived carbon with a hollow-on-hollow architecture could efficiently catalyze transfer hydrogenation of nitrobenzene [23]. Zhu et al. reported that metal-N_3 single-atom catalysts with different metal active centers achieved the reduction of nitroaromatic compounds under mild conditions [24–26]. Huang et al. also synthesized the asymmetric Cu_1-N_3 single-atom catalyst for achieving selective hydrogenation of CO_2 to obtain CO at low temperature [27]. These progresses show that the metal-N_x single-atom catalyst has a good potential in the selective reductive amination reaction. Therefore, at least three challenges need to be addressed for achieving efficient reductive amination of 4-vinylbenzaldehyde to 4-vinylbenzylamine: (1) single-atom catalyst requires a strong reducing amination capacity to ensure high conversion and stability. (2) Under catalytic reductive amination conditions, the vinyl group in 4-vinylbenzaldehyde must be suppressed to form ethyl group. (3) It is necessary to prevent the reductive coupling of 4-vinylbenzylamine and 4-vinylbenzaldehyde to form dibenzyl amine.

Owing to the specific structural asymmetry in Co single-atom

* Corresponding author.
E-mail address: djtao@jxnu.edu.cn (D.-J. Tao).
[1] The authors contribute equally to this work.

https://doi.org/10.1016/j.cej.2023.148330
Received 25 October 2023; Received in revised form 17 December 2023; Accepted 22 December 2023
Available online 27 December 2023

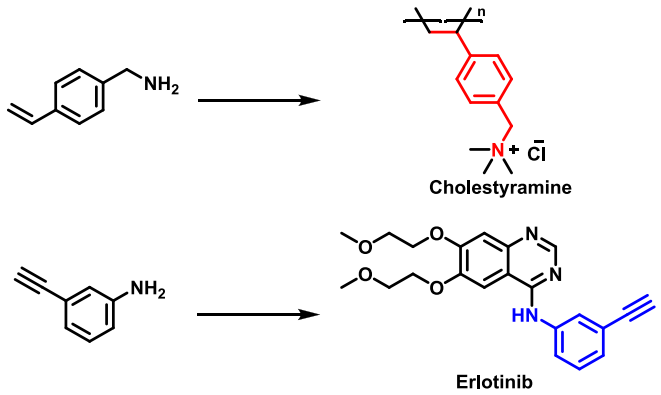

Fig. 1. Selected examples of current drugs and bio-active functionalized amines.

catalyst, Zhai and his coworkers [28] found that the asymmetric Co_1-N_2-C_2 structure could induce superior selectivity for photocatalytic oxidation CH_4 to CH_3OH. In comparison with the N atoms of Co_1-N_4 site, the asymmetric Co_1-N_2-C_2 structure could enable the charge transfer from coordinated C atoms to N atoms via the Co–C and Co–N bonds, resulting in such favorable photocatalytic activity. In addition to the regulation of single metal atom coordination environment by the C atoms, the introduction of other coordinated atoms (e.g., oxygen [29], sulfur [30], and phosphorus [31]) for boosting the catalytic activity is an attracting strategy and has received much attention.

Herein, N-doped hollow porous carbon spheres loaded with the asymmetric Co_1-N_3-O_1 single-atom were prepared by high temperature pyrolysis and subsequent acid etching. Then the reductive amination and reduction reactions over the Co_1-N_3-O_1 catalyst for highly efficient synthesis of unsaturated benzylamines and arylamines were investigated systematically. Various characterizations techniques, control experiments, and density functional theory (DFT) calculation were further carried out to clarify the paths and mechanisms of those reactions. In addition, the applicability and reusability of the Co_1-N_3-O_1 catalyst were also tested.

2. Experimental section

2.1. Materials

Cobalt(II) acetylacetonate ($Co(acac)_2$, 97 %), ammonium hydroxide solution (28 % in water), dopamine hydrochloride (99 %), tetraethoxysilane (TEOS, 99 %), cobalt phthalocyanine (CoPc, 99 %), dicyandiamide (98 %), 4-vinylbenzaldehyde (97 %), and methanol (99.5 %) were purchased from Shanghai Titan Scientific Co., Ltd. NH_3 and H_2 with a grade of 99.99 v/v% were supplied from Jiangxi Huahong Gas Co., Ltd. All chemicals and solvents were used directly without further purification.

2.2. Catalyst preparation

As shown in Scheme 1, silicon spheres were prepared by traditional Stöber method [32]. 8 mL of ammonia hydroxide solution was added to 100 mL of ethanol and 20 mL of water. Then 5 mL of TEOS was added into the above solution and stirred for 12 h to form silicon spheres. After that, 0.029 g of $Co(acac)_2$ and 0.5 g of dopamine hydrochloride were charged into the above silicon spheres solution and stirred for 10 min. A black mixture was thus formed and stirred for 12 h. After centrifugal filtration and washed to neutral, the precipitate was dried at 70 °C for 12 h to obtain a brown powder. The brown powder was put into a tubular furnace and calcined from room temperature to 900 °C under N_2 at a heating rate of 3 °C/min for 3 h. After cooling to room temperature, the obtained black powder was washed with 10 wt% hydrofluoric acid (HF) to remove the silica sphere template. Finally, the black powder was dried in a vacuum oven at 80 °C, and then the carbon spheres supported single Co atom catalyst was obtained and named as Co_1-N_3-O_1.

The synthesis procedure of N-doped carbon spheres (NC) was similar to that of Co_1-N_3-O_1, except for the addition of $Co(acac)_2$. The NC supported Co nanoparticles (Co_{NPs}) was prepared via the impregnation method using $Co(NO_3)_2{\cdot}6H_2O$ and NC, followed by the reduction of 10 % H_2/90 % N_2 (v/v) at 900 °C for 2 h. For comparison, single Co atom catalyst with the symmetric structure of Co_1-N_4 was also prepared by pyrolysis of the precursor CoPc reported in the previous reference [33].

2.3. General procedure

Typically, 0.5 mmol of aldehyde or ketone, 0.03 g of catalyst and 5 mL of methanol were added to a Teflon-lined stainless reactor and stirred for 10 min. The air in the reactor was removed by H_2, and then 1 bar NH_3 and 3 bar H_2 were injected. The reaction was performed at specified temperature and time with stirring at 800 rpm. The reduction of nitro compounds was similar to the above-mention procedure, but without filling with NH_3. After the completion of reaction, ethylbenzene was used as internal standard in the mixture. The liquid product was separated by filtration and analyzed using a Thermo Trace 1310 gas chromatography (GC) instrument equipped with FID and a TG-5HT capillary column (30 m × 0.25 mm × 0.25 μm). The molecular structures of the liquid products were identified by gas chromatography–mass spectrometry (GC–MS) (Thermo Trace 1300 GC-ISQ).

2.4. Computational details

All the DFT calculations are performed by the Vienna Ab initio Simulation Package (VASP) [34] with the projector augmented wave (PAW) method [35]. The exchange-functional is treated using the generalized gradient approximation (GGA) with Perdew-Burke-Ernzerhof (PBE) [36] functional. The energy cutoff for the plane wave basis expansion was set to 400 eV. Partial occupancies of the Kohn–Sham orbitals were allowed using the Gaussian smearing method and a width of 0.2 eV. The local structure of Co_1-N_4, Co_1-N_3-O_1, and Co_{NPs}

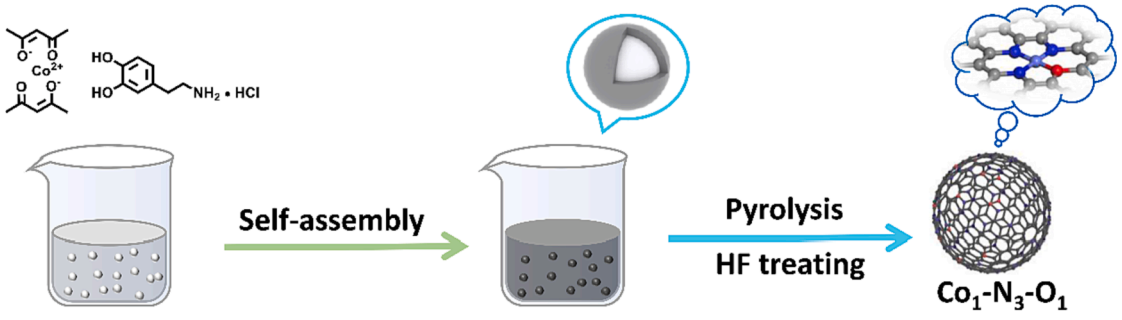

Scheme 1. Schematic illustration for the catalyst preparation of Co_1-N_3-O_1.

were built on the plane structure of graphene, where the k-point of 2 × 2 × 1 was used in all the calculations. The transition state was calculated using the constrained optimization [37]. The self-consistent calculations apply a convergence energy threshold of 10^{-4} eV, and the force convergency was set to 0.05 eV/Å. The free energy corrections were considered at the temperature of 358 K, following:

$$\Delta G = \Delta E + \Delta G_{ZPE} + \Delta G_U - T\Delta S$$

where ΔE, ΔG_{ZPE}, ΔG_U, and ΔS refer to the DFT calculated energy change, the correction from zero-point energy, the correction from inner energy and the correction from entropy [38].

3. Results and discussion

3.1. Catalyst preparation and characterization

The XRD and XPS patterns of the catalyst precursor were shown in Figure S1, indicating that cobalt has been loaded on the precursor. The metallic Co mass contents in the Co_1-N_3-O_1, Co_1-N_4, and Co_{NPs} catalysts were tested by inductively coupled optical emission spectrometer and the results are listed in Table S1. It is found that the Co mass percentage of Co_1-N_3-O_1 was 0.78 wt%, as well as the Co mass percentage of Co_1-N_4 was 0.91 wt%. For comparison, the Co_{NPs} catalyst had the highest metallic Co content of 6.74 wt%. Moreover, the crystal phases of the catalyst samples were characterized by X-ray diffraction (XRD) (Figure S2). Two characteristic peaks appeared near 25° and 43°, which belong to the (002) and (100) crystal planes of graphite-like carbon [39], respectively. Three peaks at 2θ=44.2°, 51.5°, and 75.9° were observed in the XRD pattern of Co_{NPs}, assigned to the (111), (200), and (220) crystal planes of metallic Co^0 (PDF#15-0806). The crystal diffraction peaks of metallic Co^0 were not found in Co_1-N_3-O_1 and Co_1-N_4, showing the probable absence of Co nanoparticles in these two catalysts.

Scanning electron microscope (SEM) image showed that the shape of the hollow porous carbon spheres was uniform (Fig. 2a). Transmission electron microscope (TEM) images also indicated that the diameter of hollow porous carbon spheres was around 100 nm, and the surface was distributed with a thick-layered structure (Fig. 2b & c). The Co nanoparticles and clusters were not observed for the Co_1-N_3-O_1 catalyst, which is consistent with the XRD results (Figure S2). Similarly, the TEM images of Co_1-N_4 showed carbon layered nanostructures without the observation of Co nanoparticles (Figure S3). By comparing the TEM images before and after HF treatment (Fig. 2b ~ d), it is demonstrated that the carbon sphere was hollow and the surface was not damaged by HF. Moreover, the aberration-corrected high-angle annular dark-field scanning transmission electron microscopy (AC-HAADF-STEM) images (Fig. 2e & f) indicated that the surface of hollow porous carbon spheres was covered with a thin layer containing Co single atoms (the bright spots as shown in Fig. 2g, Figure S4). Energy dispersion spectroscopy (EDS) mapping was further used to test the distribution of major elements on the surface of Co_1-N_3-O_1 catalyst. Fig. 2h ~ k show that the Co, N and O elements were uniformly distributed on the surface of hollow porous carbon spheres. Especially, the weak signal of Co mapping in the Co_1-N_3-O_1 catalyst with highly dispersing uniform state further verifies

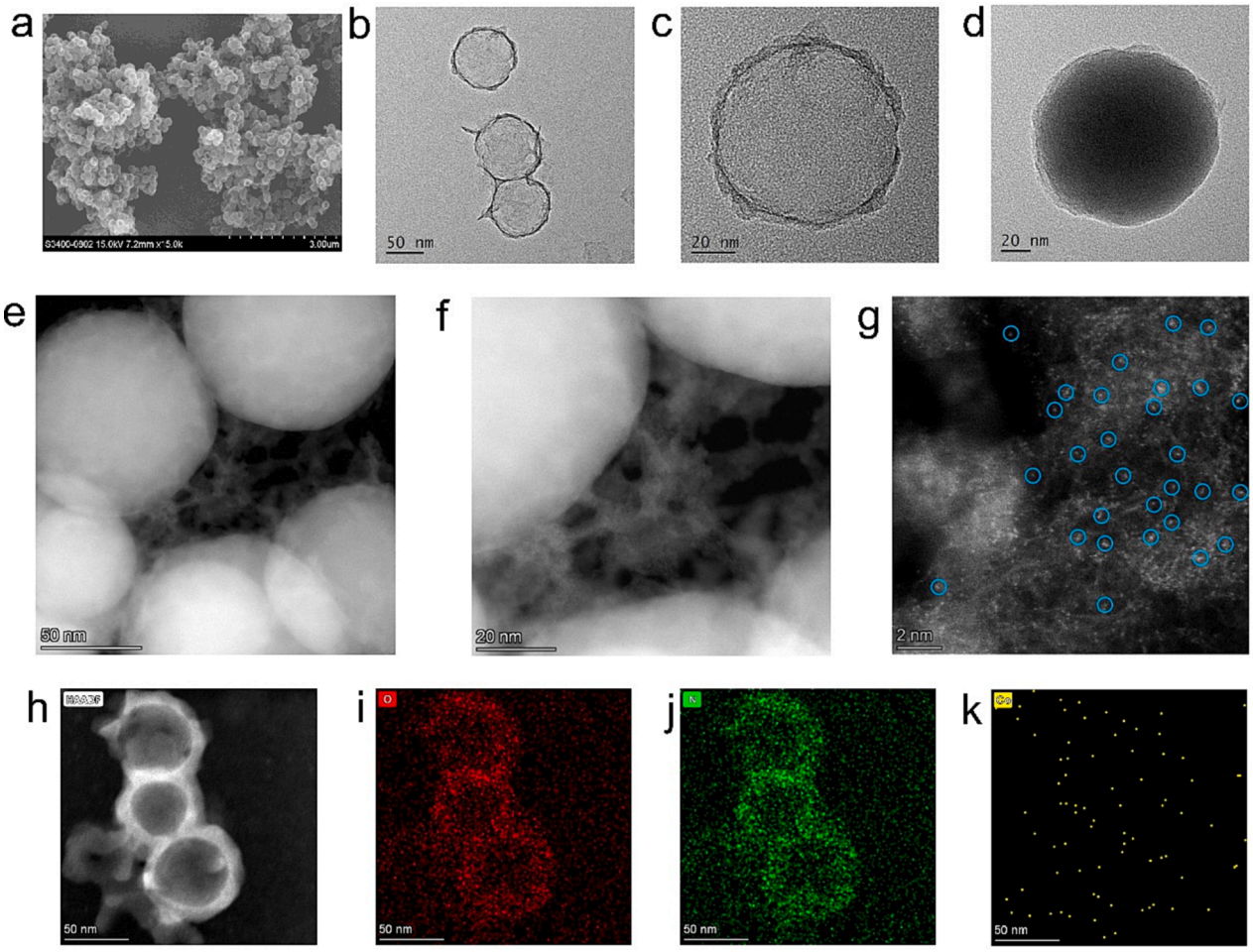

Fig. 2. (a) SEM image and (b & c) TEM images of Co_1-N_3-O_1; (d) TEM image of Co_1-N_3-O_1 before HF treating; (e ~ g) AC-HAADF-STEM images, (h ~ k) EDS mapping of Co_1-N_3-O_1.

the presence of Co single atoms in the Co_1-N_3-O_1 catalyst.

The surface areas and pore volumes of the samples were tested by the N_2 adsorption/desorption isotherms (Fig. 3a, Figure S5). The Brunauer–Emmett–Teller (BET) surface area and pore volume of Co_1-N_3-O_1 catalyst were calculated to be 788 m^2/g and 2.94 cm^3/g, which are slightly smaller than those of NC without Co loading (surface area of 863 m^2/g, pore volume of 3.59 cm^3/g) (Table S1). Whereas, the BET surface area of Co_{NPs} decreased significantly to 562 m^2/g due to the aggregation of a large amount of Co nanoparticles. Additionally, the surface area of Co_1-N_4 catalyst was only 88 m^2/g and much lower than that of Co_1-N_3-O_1. This shows that silicon sphere as a sacrificial template can result in the large surface area.

X-ray photoelectron spectroscopy (XPS) was used to measure the elemental and valence composition of the catalyst surface. Table S2 lists the results of the C, N, O element content in the surface of Co_1-N_3-O_1. The binding energies at 778.6 eV and 793.7 eV in the Co 2p XPS spectra confirmed the presence of Co nanoparticles in the Co_{NPs} catalyst (Fig. 3b), while these two peaks were not found in the Co_1-N_3-O_1 and Co_1-N_4 catalysts, which are accordance with the above XRD and TEM results. Moreover, the peaks with the binding energies of 780.7 eV and 796.1 eV could be fitted in the Co 2p XPS spectra, which is assigned the Co^{2+} species [40]. Fig. 3c shows the N 1s spectra of the Co_1-N_3-O_1 and Co_1-N_4 catalysts. It is found that graphitic N (401.3 ~ 401.4 eV) was mainly in Co_1-N_3-O_1, while Co_1-N_4 had more pyridinic N (398.5 ~ 398.7 eV). A fitting peak at 399.6 eV attributing to the Co-N_x bond was simultaneously detected in the Co_1-N_3-O_1 and Co_1-N_4 catalysts [41]. In addition, the O 1s XPS spectra of the Co_1-N_3-O_1 and Co_{NPs} catalysts were fitted into four peaks as follows: O=C (531 eV), O-C (532.1–532.4 eV), O=C-OH (533.5–533.8 eV) and O-Co (530.3 eV) (Fig. 3d) [42]. The fitting peak of O-Co was absent in the Co_1-N_4 catalyst, verifying the coordination of Co atom with N atoms in the Co_1-N_4 catalyst.

X-ray absorption fine structure (XAFS) measurements at the Co K-edge were performed to investigate the local structures of Co species in the Co_1-N_3-O_1 catalyst. The normalized X-ray absorption near-edge structure (XANES) results are shown in Fig. 4a. Compared with the standard Co foil, the absorption edge of Co_1-N_3-O_1 shifts to the higher energy and is close to that for CoO, indicating that the valence state of Co in Co_1-N_3-O_1 should be close to + 2. The R space of the Fourier transform K^2-weighted extended X-ray absorption fine structure (FT-EXAFS) spectra of Co_1-N_3-O_1 showed that the main peak of Co_1-N_3-O_1 at 1.41 Å was attributed to the Co-N or Co-O bond (Fig. 4b) [43], which is shorter than the Co–O peak of the standard CoO and the Co–Co peak of the standard Co foil. No Co–Co peaks or other high-shell peaks were observed for Co_1-N_3-O_1, again confirming the single atom dispersion of Co species in the Co_1-N_3-O_1.

Subsequently, Fig. 4c ~ e shows the wavelet transforms (WTs) of Co K-edge EXAFS oscillations. The contour plots of Co_1-N_3-O_1 present only one intensity maximum at ~ 1.41 Å (Y-axis) assigning to Co–N or Co–O coordination, as well as no intensity maximum related to Co–Co coordination is detected. These findings obviously demonstrate that the Co species in Co_1-N_3-O_1 are coordinated by N and O atoms. Furthermore, the precise coordination configuration of Co single-atom was correlated

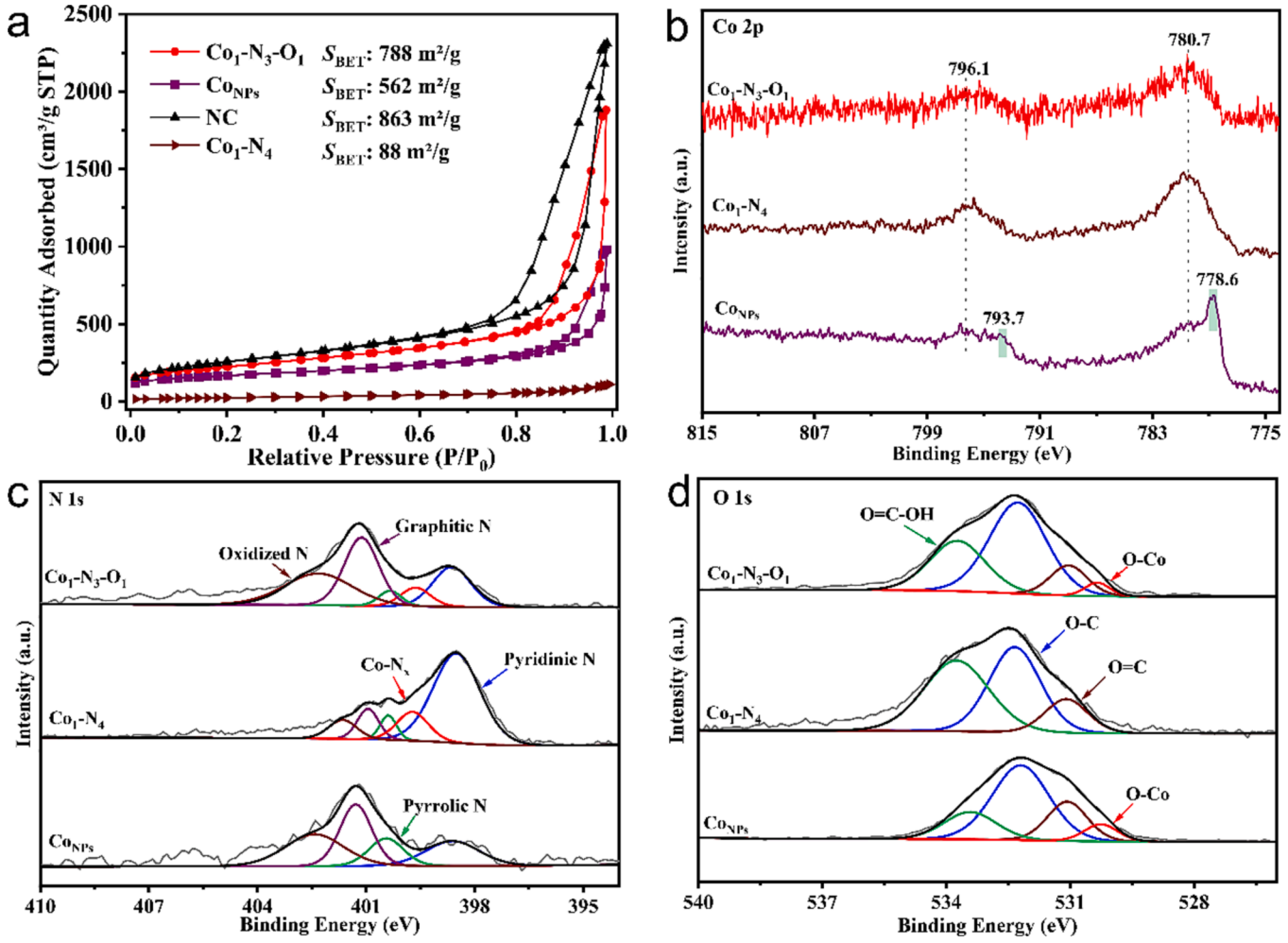

Fig. 3. (a) N_2 adsorption–desorption isotherms of the Co_1-N_3-O_1, Co_1-N_4, Co_{NPs}, and NC catalysts; (b) Co 2p, (c) N 1s, and (d) O 1s XPS spectra of the Co_1-N_3-O_1, Co_1-N_4, and Co_{NPs} catalysts.

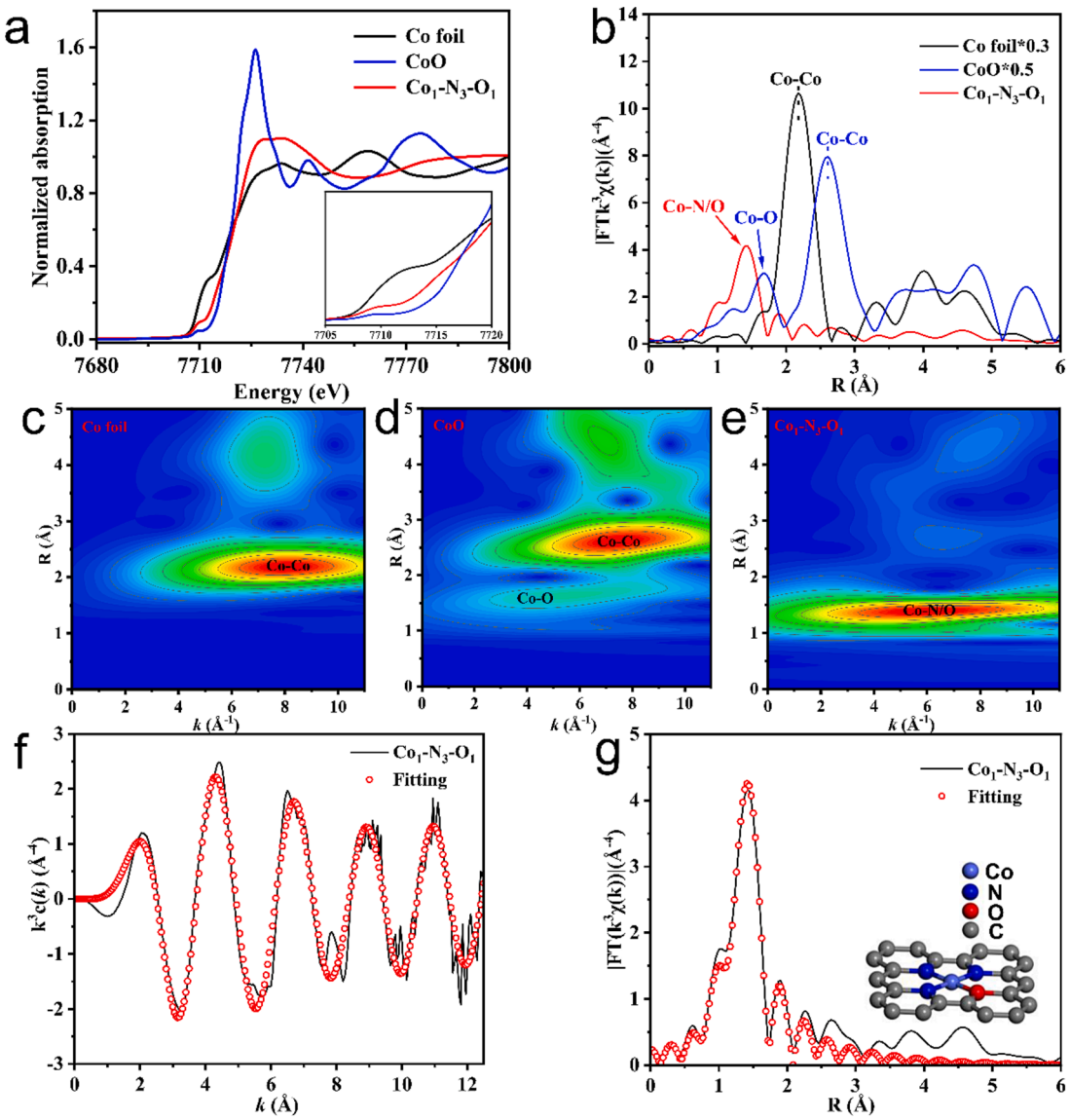

Fig. 4. (a) Co K-edge XANES spectra, (b) FT k^3-weighted EXAFS spectra of Co foil, CoO and Co_1-N_3-O_1; (c ~ e) Wavelet-transformed k^3-weighted EXAFS spectra of Co foil, CoO and Co_1-N_3-O_1; (f) Co K-edge EXAFS fitting caves in k space; (g) Co K-edge EXAFS fitting caves in R space.

Table 1
Catalyst screening for the reductive amination of 4-vinylbenzaldehyde.[a]

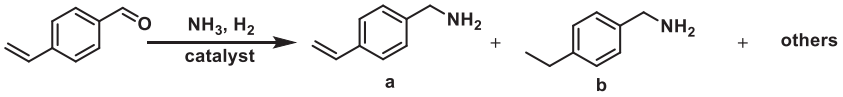

Entry	Catalyst	Conversion (%)	Selectivity (%)		
			a	b	others
1	Co_1-N_3-O_1	>99	>99	0	0
2	Co_1-N_4	>99	47	31	22
3	Co_{NPs}	>99	20	62	18
4	NC	>99	0	0	>99
5	CoPc	>99	0	0	>99
6	$Co(acac)_2$	>99	0	0	>99
7	Pd/C	>99	0	68	32
8	Ru/Al_2O_3	>99	12	33	55
9[b]	Co_1-N_3-O_1	>99	>99	0	0

[a] Reaction conditions: 4-vinylbenzaldehyde (0.5 mmol), catalyst (30 mg), NH_3 (1 bar), 120 °C, H_2 (3 bar), methanol (5 mL), 2 h, 800 rpm. [b]60 °C, 4 h.

by FT-EXAFS fitting of the first shell, and the fitting results for different Co coordination environments were shown in Table S3, Figures S6 and S7. It is found that the configuration model of Co_1-N_3-O_1 shows the best k space and R space fitting results (Fig. 4f & g). The coordination number of the central Co atom is about 4, while the mean Co–N bond and Co–O bond length of Co_1-N_3-O_1 are 1.89 Å and 2.06 Å, respectively (Table S3).

As a result, the four-coordinated Co atomic structure is shown in the inset of Fig. 2g, in which each single Co atom is coordinated by three N atoms and one O atom in the plane.

3.2. Catalyst screening

Considering that the vinyl and aldehyde groups are easily reduced, the reductive amination of 4-vinylbenzaldehyde with higher chemoselectivity to generate 4-vinylbenzylamine was challenging due to the occurrence and competition of various side-reactions (Figure S8). To our great delight, the Co_1-N_3-O_1 catalyst exhibited the highest selectivity to 4-vinylbenzylamine with almost quantitative yield through reductive amination of 4-vinylbenzaldehyde at 120 °C for 2 h under 1 bar NH_3 and 3 bar H_2 (Table 1, entry 1). However, both of the Co_1-N_4 and Co_{NPs} catalysts showed very low selectivities of 4-vinylbenzylamine (Table 1, entries 2, 3), indicating that the over-reduction of vinyl group and other side reaction occurred to 4-ethylbenzylamine, bis(4-ethylbenzyl)amine and *N*-(4-ethylbenzyl)-1-(4-ethylphenyl)methanimine (Figure S8). In the poisoning experiments using KSCN and thiophene (Table S4), KSCN exhibited a strong inhibitory effect on formation of 4-vinylbenzylamine compared with thiophene, indicating that the catalyst activity is derived from Co single atoms rather than Co nanoparticles or clusters. This is because that KSCN has a strong affinity to Co single atoms and thereby cause the loss of catalytic activity [44]. On NC catalyst, 4-vinylbenzaldehyde and NH_3 were dehydrated and condensed to form imine and their dimers. No catalytic activity was found on NC, which indicates that cobalt was crucial species in the reaction (Table 1, entry 4). The catalytic performance of Co_1-N_3-O_1 was also better than other cobalt-based homogeneous catalysts. Homogeneous CoPc and $Co(acac)_2$ were unable to catalyze this transformation in the reductive amination of 4-vinylbenzaldehyde (Table 1, entries 5 and 6). Pd/C and Rh/Al_2O_3 with stronger reducing ability showed low selectivity, and other by-products were 4-methylethylbenzene and 4-ethylbenzyl alcohol (Table 1, entries 7 and 8). The mass spectra of the main product and by-products were shown in Figure S9. Particularly, the Co_1-N_3-O_1 catalyst still induced a 99 % yield of 4-vinylbenzylamine at a relatively low temperature of 60 °C for 4 h (Table 1, entry 9). To verify whether over-reduction occurs at longer reaction time, the experiment with longer reaction time was conducted. After 12 h of reaction at 120 °C, there was still 99 % selectivity of 4-vinylbenzylamine over the Co_1-N_3-O_1 catalyst, but 4-ethylbenzylamine and bis(4-ethylbenzyl)amine were the main products using the Co_1-N_4 and Co_{NPs} catalysts (Figures S10 and S11).

Then, the reaction conditions for reductive amination of 4-vinylbenzaldehyde catalyzed by the Co_1-N_3-O_1 catalyst were optimized. Solvent was one of the most important factors for the liquid-phase catalytic reaction (Table S5). Better catalysis was observed in protic solvents, where methanol was able to exhibit the highest selectivity to 4-vinylbenzylamine. Yields were greatly affected in polar aprotic solvents, and the conversions were reduced in nonpolar solvents. In many heterogeneous catalytic reduction systems, the critical role of alcohols in heterolytic cleavage of H_2 molecules by H-shuttling mechanism has been demonstrated [19,45]. The methanol molecule accepts an activated H atom from the Co site and meanwhile donate a H atom to the acceptor by hydrogen bond, thereby promoting the heterolytic cleavage of H_2 [46]. Protic solvent mediated hydrogen transfer generally has a lower activation barrier, leading to a significant enhancement of hydrogenation activity in the presence of alcohols [47]. The yield of 4-vinylbenzylamine performed a positive correlation with the H_2 pressure from 1 bar to 12 bar, with slowly increase after 3 bar probably because the H_2 concentration was already sufficient to cover almost the entire catalyst surface (Table S6). Unlike H_2 pressure and solvents, NH_3 pressure showed no such significant influence on the reductive amination of 4-vinylbenzaldehyde, since there was enough NH_3 to dehydrate and condensation with carbonyl group to form –CH=NH bond because of the excellent solubility (Table S7). The hydrogen source also had influence in reductive amination. H_2, formic acid, and hydrazine hydrate were used as hydrogen sources respectively. The catalyst exhibited the highest 4-vinylbenzylamine yield under H_2 condition, whereas formic acid and hydrazine hydrate showed poor catalytic activity (Table S8). No activity of formic acid as hydrogen source was due to the reaction of formic acid with ammonia to form ammonium formate. For hydrazine hydrate, it was difficult to catalyze the decomposition of hydrazine hydrate at low temperatures. In order to investigate the stability and reusability of Co_1-N_3-O_1, the catalyst was tested at 50 °C and separated by simple centrifugation. After recycled for 10 times, the yield was still higher than 20 % (Figure S12), implying the reliable durability of the Co_1-N_3-O_1 catalyst. From the XRD, EDS, N_2 adsorption–desorption curve and XPS characterization results of the recycled catalyst (Figure S13), it can be found that single Co atoms did not agglomerate to form Co nanocrystals. The morphology, specific surface area, surface element distribution and valence state of the catalyst did not obvious change. These all indicate that the catalyst has good stability.

3.3. Reaction mechanism investigations

Above experimental results showed that the reductive amination of 4-vinylbenzaldehyde over the Co_1-N_3-O_1 catalyst mainly leaded to 99 % yield of 4-vinylbenzylamine, while the Co_1-N_4 and Co_{NPs} catalysts produced a large amount of 4-ethylbenzylamine. To reveal the intrinsic catalytic mechanism, DFT was employed to probe the hydrogenation behavior of intermediate product (4-vinylphenyl)methanimine (containing both vinyl and imine unsaturated functional groups) on different catalysts. Firstly, the hydrogenation process of (4-vinylphenyl)methanimine molecule adsorbed on Co_1-N_3-O_1 and Co_1-N_4 surface with C=N terminal was calculated. The energy profiles are shown in Fig. 5a, and corresponding structures including transition state (TS) and intermediate state are shown in Figures S14 and S15. It can be seen from Fig. 5a that the process of (4-vinylphenyl)methanimine adding the first H atom possesses the highest energy barrier, which is the rate-controlling step. The TS1 energy barrier of Co_1-N_3-O_1 is 0.17 eV lower than that of Co_1-N_4, and its TS2 energy barrier is also 0.05 eV lower. This indicates the imine group on (4-vinylphenyl)methanimine is more easily reduced to amino group by hydrogenation on Co_1-N_3-O_1. Additionally, the hydrogenation behavior of (4-vinylphenyl)methanimine adsorbed on Co_1-N_3-O_1, Co_1-N_4 and Co_{NPs} with the terminal C=C double bond was further investigated. The energy changes is shown in Fig. 5b, and corresponding calculated structures are shown in Figures S16 ~ S18. From Fig. 5b, it can be observed the two-step hydrogenation energy barriers (2.44 eV and 1.25 eV) of C=C on Co_1-N_3-O_1 are the highest, while the energy barriers of TS1 and TS2 on Co_1-N_4 are 1.19 eV and 0.76 eV, and these on Co_{NPs} are 0.75 eV and 0.97 eV, respectively. The highest hydrogenation energy barrier of C=C on the three catalysts is in the order of Co_1-N_3-O_1 > Co_1-N_4 > Co_{NPs}, which maks a good agreement with the sequence of the yield of by-product 4-ethylbenzylamine. In particular, the TS1 energy barrier on Co_1-N_3-O_1 is about twice that of Co_1-N_4, which implies (4-vinylphenyl)methanimine is more difficult to implement C=C hydrogenation on Co_1-N_3-O_1.

The faster H_2 dissociation rate is beneficial to increase the hydrogenation rate, but it will also increase the reduction tendency of various unsaturated functional groups. Therefore, the dissociation barriers of H_2 on the surface of Co_1-N_4, Co_1-N_3-O_1 and Co_{NPs} were also investigated. The energy change of the dissociation process and the corresponding state structures are shown in Figures S19 ~ S22. It can be seen from Figure S19 that the dissociation energy barrier of H_2 on Co_{NPs} is the lowest (0.45 eV), followed by Co_1-N_4 (1.72 eV), and the highest is Co_1-N_3-O_1 with 2.23 eV. This shows that during the hydrogenation reaction, the concentration of surface dissociated H is very probably the highest on Co_{NPs}, which would result in the highest reduction tendency of various unsaturated functional groups on it. On the contrary, the degree of H_2 dissociation on the surface of Co_1-N_3-O_1 is not so violent, which is beneficial to suppress other competing hydrogenation reactions.

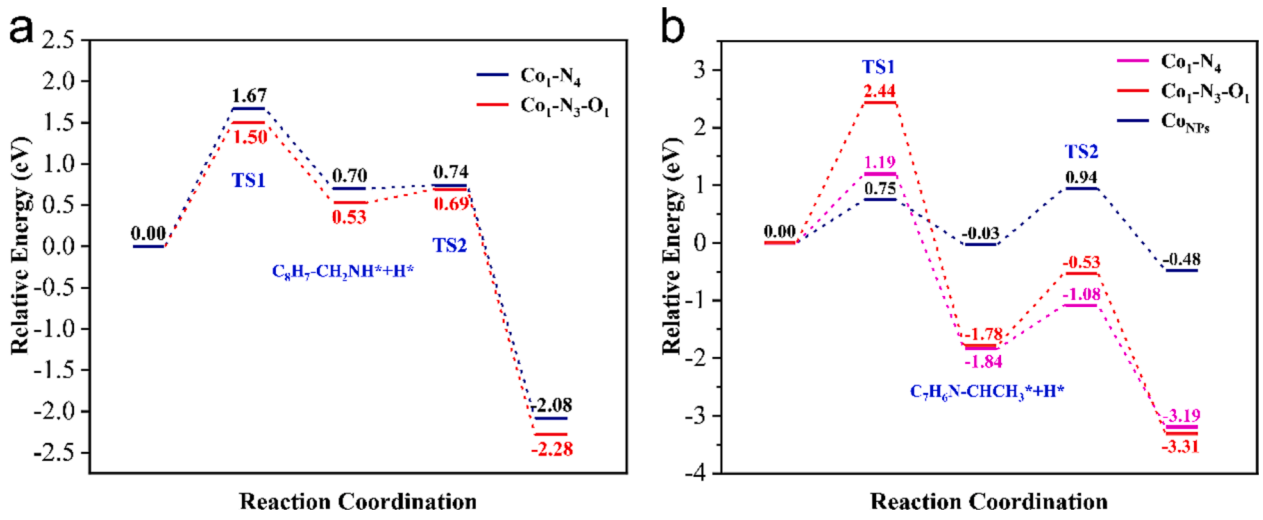

Fig. 5. (a) Energy profiles of (4-vinylphenyl)methanimine hydrogenation by C=N on Co_1-N_4, and Co_1-N_3-O_1 surface; (b) Energy profiles of (4-vinylphenyl)methanimine hydrogenation by C=C on Co_1-N_4, Co_1-N_3-O_1 and Co_{NPs} surface.

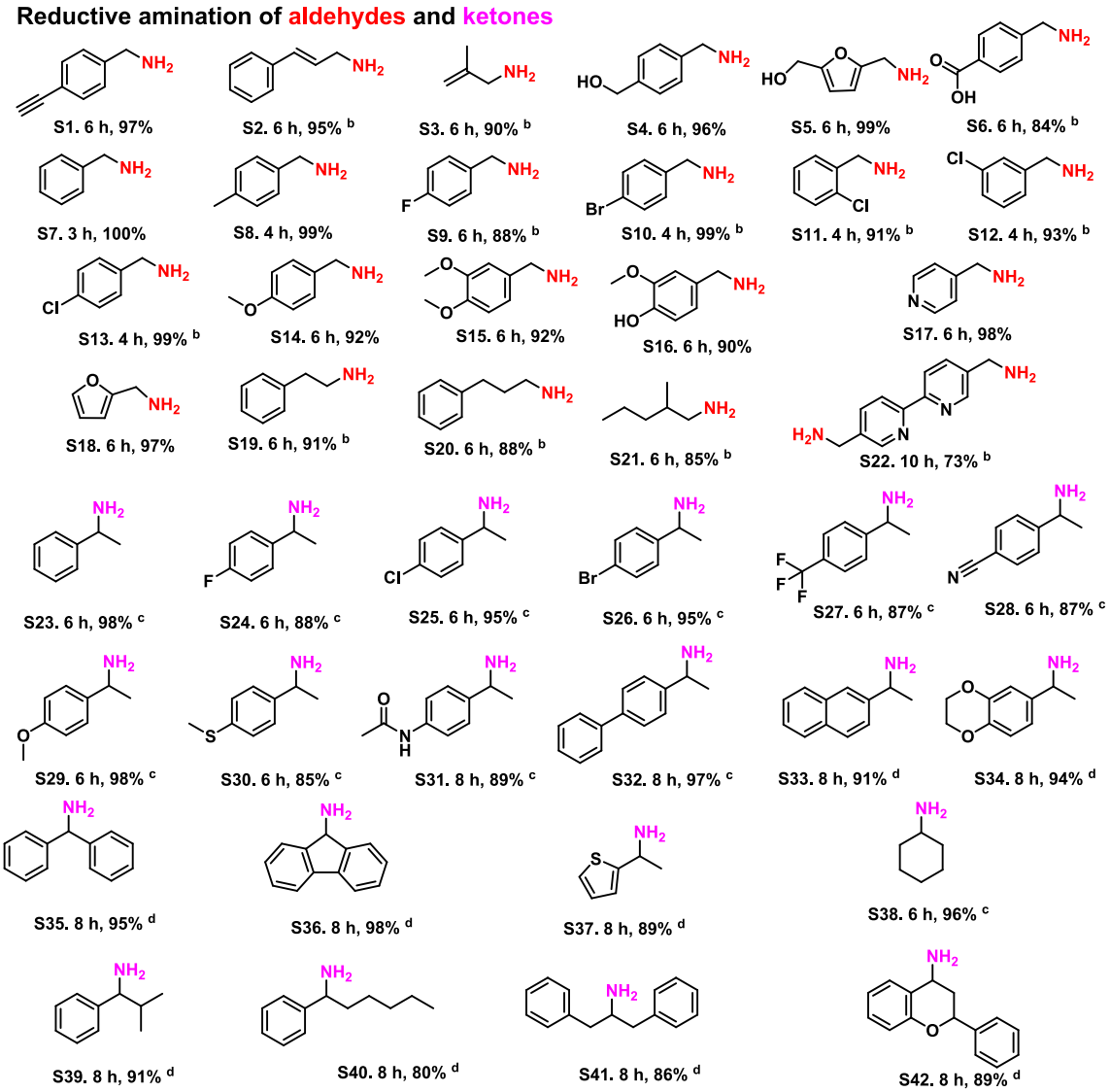

Fig. 6. Reductive amination of aldehydes and ketones with different substituted groups. [a] Conditions: substrate (0.5 mmol), catalyst (30 mg), 60 °C, NH_3 (1 bar), H_2 (3 bar), methanol (5 mL), 800 rpm. [b] 90 °C; [c] 100 °C; [d] 120 °C.

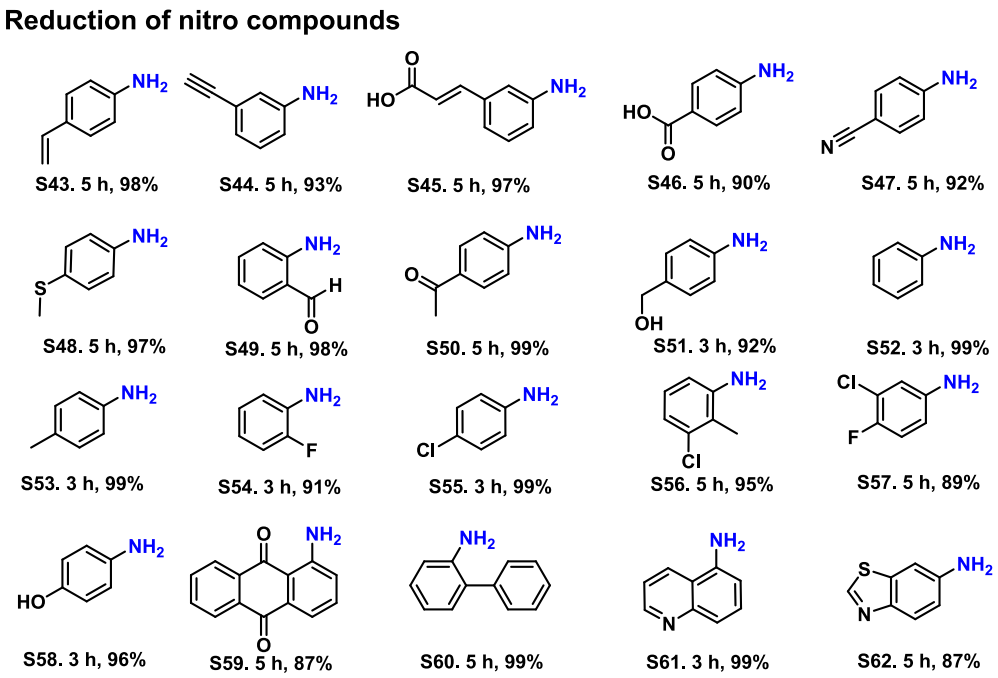

Fig. 7. Reduction reactions of nitro compounds with different substituted groups. Conditions: substrate (0.5 mmol), catalyst (30 mg), 60 °C, H_2 (3 bar), methanol (5 mL), 800 rpm.

3.4. Substrate scope

Various amines obtained by the reductive amination of aldehydes or ketones are very useful for the synthesis of drugs, pesticides and functional materials. Then the Co_1-N_3-O_1 catalyst was further applied to the reductive amination of different types of aldehydes including aromatic and aliphatic aldehydes. As shown in Figs. 6, 4- acetenylbezaldehyde was completely transformed to 4-acetenylbenzylamine (S1) at 60 °C and 6 h. Cinnamamine (S2) was conveniently formed by reductive amination of cinnamaldehyde. For unsaturated aliphatic amine, 2-methylallylamine (S3) was synthesized from 2-methacrolein at 90 °C. The synthesis of some amines containing sensitive functional groups can be also efficiently synthesized. For example, hydroxyl groups (S4-S5) and carboxyl group (S6) are well preserved during reductive amination. Benzaldehyde and its alkyl substitutes (S7-S8), as the most basic aromatic aldehydes, are completely converted to corresponding benzylamines at 60 °C. Benzaldehyde with F-, Cl- and Br-substituents (S9 ~ S13) can be reduced to corresponding benzylamines. Benzaldehyde substrates containing electron-donating functional groups (such as hydroxyl, methoxy and their disubstituted groups) also achieved high yields (S14 ~ S16). Heterocyclic aldehydes containing pyridine (S17) and furan rings (S5, S18) can be used to synthesize their corresponding primary amines, which can be used as valuable precursors and intermediates in the field of life sciences. The key psychotropic drug monomers phenylethylamine (S19) and amphetamine (S20) were obtained with more than 88 % yield. Also, 2-methylpentylamine and 5,5′-bis(aminomethyl)-2,2′-bipyridine were efficiently realized from alkyl and pyridinic aldehydes (S21, S22).

In addition to aromatic aldehydes, the Co_1-N_3-O_1 catalyst was also be efficiently applied to reductive amination of aromatic ketones. Acetophenone and its halogen-, cyano-, methoxy-, methylthio-, and amide functional group-substituted analogues exhibited high activity (S23-S31), demonstrating higher chemoselectivity and sulfur tolerance of Co_1-N_3-O_1. As expected, the fuse-ring ketones and aryl-aryl ketone (S32-S36) with large steric hindrance required high reaction temperature of 120 °C to obtain the target amine products with high yields. Acetyl thiophene and cyclohexanone can be reductively aminated to obtain corresponding amines (S37, S38). Besides, aryl–alkyl (cyclic) ketones were also successfully reduced to the destination amines (S39-S42).

Following the success of reductive amination of aldehydes/ketones, the hydrogenation of nitrobenzene with different substituted functional groups over the Co_1-N_3-O_1 catalyst was explored (Fig. 7). As an important intermediate of antitumor agent Icotinib and Erlotinib [48], 4-vinylaniline (S43) and 3-aminophenylacetylene (S44) were obtained with more than 93 % yield. A 90 % yield of 3-aminocinnamic acid (S45) was also realized. Moreover, nitrobenzenes bearing different functional groups (e.g., –COOH, $–CH_3$, halogen, –CN, –OH, $-SCH_3$ and –CHO) were efficiently converted to corresponding anilines (S46 ~ S58). In addition, four anilines containing fused rings and heterocycles (S59 ~ S62) were also received with excellent yields. Overall, the Co_1-N_3-O_1 catalyst exhibited fascinating catalytic activities in a wide scope of synthetic various anilines, demonstrating its universal applicability.

4. Conclusion

In summary, hollow N-doped carbon nanospheres supported Co single atoms with an asymmetric Co_1-N_3-O_1 structure was successfully prepared and characterized. The Co_1-N_3-O_1 catalyst exhibited good performance for efficient synthesis of various unsaturated benzylamines and arylamines from unsaturated aldehydes and nitro compounds under mild conditions. Compared with the indiscriminate activation cases of Co_1-N_4 and Co_{NPs}, the Co_1-N_3-O_1 catalyst had the highest hydrogenation energy barrier of the terminal C=C bond, which is beneficial to suppress competing hydrogenation reactions and thereby results in excellent yields of unsaturated benzylamines and arylamines. Therefore, the asymmetrically structured Co single-atom catalyst is considered to be an encouraging catalyst for highly efficient and selective reductive amination reaction.

Author Contributions

D.T. conceived the initial idea and experimental design. S.H. carried out and analyzed the experiments. M.S. carried out the DFT calculations. W.C., and Y.Z. contributed to the data analyses. All authors discussed the results and commented on the manuscript. S.H., M.S. and D.T. wrote the paper with help from all authors. #S.H and M.S. contributed equally.

CRediT authorship contribution statement

Song Han: Data curation, Investigation, Methodology, Writing – original draft. **Ming-Shuai Sun:** Data curation, Methodology, Resources, Software, Writing – review & editing. **Wen-Ting Chen:** Methodology, Resources. **Yan Zhou:** Methodology, Resources. **Duan-Jian Tao:** Conceptualization, Project administration, Resources, Supervision, Writing – review & editing.

Declaration of competing interest

The authors declare that they have no known competing financial interests or personal relationships that could have appeared to influence the work reported in this paper.

Data availability

Data will be made available on request.

Acknowledgment

We thank the Key Lab of Fluorine and Silicon for Energy Materials and Chemistry of Ministry of Education, Jiangxi Normal University (KFSEMC-202209) and the National Natural Science Foundations of China (22378178) for financial support. Song Han thanks the Scientific Research Foundation of Graduate Innovation of Jiangxi Normal University (YJS2023020) for financial support.

Appendix A. Supplementary data

Supplementary data to this article can be found online at https://doi.org/10.1016/j.cej.2023.148330.

References

[1] R.V. Jagadeesh, K. Murugesan, A.S. Alshammari, H. Neumann, M.M. Pohl, J. Radnik, M. Beller, MOF-derived cobalt nanoparticles catalyze a general synthesis of amines, Science 358 (2017) 326–332.
[2] K. Murugesan, V.G. Chandrashekhar, T. Senthamarai, R.V. Jagadeesh, M. Beller, Reductive amination using cobalt-based nanoparticles for synthesis of amines, Nat. Protoc. 15 (2020) 1313–1337.
[3] H.F. Qi, J. Yang, F. Liu, L.L. Zhang, J.Y. Yang, X.Y. Liu, L. Li, Y. Su, Y.F. Liu, R. Hao, A.Q. Wang, T. Zhang, Highly selective and robust single-atom catalyst Ru_1/NC for reductive amination of aldehydes/ketones, Nat. Commun. 12 (2021) 3295.
[4] B.X. Zheng, J. Xu, J.L. Song, H.H. Wu, X.L. Mei, K.L. Zhang, W.Y. Han, W. Wu, M. Y. He, B.X. Han, Nanoparticles and single atoms of cobalt synergistically enabled low-temperature reductive amination of carbonyl compounds, Chem. Sci. 13 (2022) 9047–9055.
[5] H.T. Zou, J.Z. Chen, Efficient and selective approach to biomass-based amine by reductive amination of furfural using Ru catalyst, Appl. Catal. b: Environ. 309 (2022), 121262.
[6] C.J. Glueck, S. Ford Jr., D. Scheel, P. Steiner, Colestipol and cholestyramine resin: comparative effects in familial type II hyperlipoproteinemia, JAMA 222 (1972) 676–681.
[7] X.C. Jv, S.T. Sun, Q. Zhang, M.Y. Du, L. Wang, B. Wang, Efficient and mild reductive amination of carbonyl compounds catalyzed by dual-function palladium nanoparticles, ACS Sustainable Chem. Eng. 8 (2020) 1618–1626.
[8] M. Manzoli, E.C. Gaudino, G. Cravotto, S. Tabasso, R.B.N. Baig, E. Colacino, R. S. Varma, Microwave-assisted reductive amination with aqueous ammonia: Sustainable pathway using recyclable magnetic nickel-based nanocatalyst, ACS Sustainable Chem. Eng. 7 (2019) 5963–5974.
[9] J.Z. Qin, B. Han, X.M. Lu, J.B. Nie, C.S. Xian, Z.H. Zhang, Biomass-derived single Zn atom catalysts: the multiple roles of single Zn atoms in the oxidative cleavage of C-N bonds, JACS Au 3 (2023) 801–812.
[10] X.F. Yang, A.Q. Wang, B.T. Qiao, J. Li, J.Y. Liu, T. Zhang, Single-atom catalysts: A new frontier in heterogeneous catalysis, Acc. Chem. Res. 46 (2013) 1740–1748.
[11] B.T. Qiao, A.Q. Wang, X.F. Yang, L.F. Allard, Z. Jiang, Y.T. Cui, J.Y. Liu, J. Li, T. Zhang, Single-atom catalysis of CO oxidation using Pt_1/FeO_x, Nat. Chem. 3 (2011) 634–641.
[12] J. Yang, H.F. Qi, A.Q. Li, X.Y. Liu, X.F. Yang, S.X. Zhang, Q. Zhao, Q.K. Jiang, Y. Su, L.L. Zhang, J.F. Li, Z.Q. Tian, W. Liu, A.Q. Wang, T. Zhang, Potential-driven restructuring of Cu single atoms to nanoparticles for boosting the electrochemical reduction of nitrate to ammonia, J. Am. Chem. Soc. 144 (2022) 12062–12071.
[13] J. Jones, H.F. Xiong, A.T. DeLaRiva, E.J. Peterson, H. Pham, S.R. Challa, G. Qi, S. Oh, M.H. Wiebenga, X.I. Pereira Hernández, Y. Wang, A.K. Datye, Thermally stable single-atom platinum-on-ceria catalysts via atom trapping, Science 353 (2016) 150–154.
[14] X. Liang, N.H. Fu, S.C. Yao, Z. Li, Y.D. Li, The progress and outlook of metal single-atom-site catalysis, J. Am. Chem. Soc. 144 (2022) 18155–18174.
[15] Y. Fan, C.F. Zhuang, S.J. Li, Y. Wang, X.Q. Zou, X.T. Liu, W.M. Huang, G.S. Zhu, Efficient single-atom Ni for catalytic transfer hydrogenation of furfural to furfuryl alcohol, J. Mater. Chem. A 9 (2021) 1110–1118.
[16] S. De, A.S. Burange, R. Luque, Conversion of biomass-derived feedstocks into value-added chemicals over single-atom catalysts, Green Chem. 24 (2022) 2267–2286.
[17] T.T. Jia, D. Meng, R. Duan, H.W. Ji, H. Sheng, C.C. Chen, J. Li, W.J. Song, J. C. Zhao, Single-atom nickel on carbon nitride photocatalyst achieves semihydrogenation of alkynes with water protons via monovalent nickel, Angew. Chem. Int. Ed. 62 (2023) e202216511.
[18] J.H. Fu, J.H. Dong, R. Si, K.J. Sun, J.Y. Zhang, M.R. Li, N.N. Yu, B.S. Zhang, M. G. Humphrey, Q. Fu, J.H. Huang, Synergistic effects for enhanced catalysis in a dual single-atom catalyst, ACS Catal. 11 (2021) 1952–1961.
[19] M.H. Li, C.C. Zhang, Y. Tang, Q.L. Chen, W. Li, Z. Han, S.Y. Chen, C.C. Lv, Y.J. Yan, Y. Zhang, W.H. Zheng, P. Wang, X.F. Guo, W.P. Ding, Environment molecules boost the chemoselective hydrogenation of nitroarenes on cobalt single-atom catalysts, ACS Catal. 12 (2022) 11960–11973.
[20] S.B. Tian, M. Hu, Q. Xu, W.B. Gong, W.X. Chen, J.R. Yang, Y.Q. Zhu, C. Chen, J. He, Q. Liu, H.J. Zhao, D.S. Wang, Y.D. Li, Single-atom Fe with Fe_1N_3 structure showing superior performances for both hydrogenation and transfer hydrogenation of nitrobenzene, Sci. China Mater. 64 (2021) 642–650.
[21] S. Liu, H.B. Yang, S.F. Hung, J. Ding, W.Z. Cai, L.H. Liu, J.J. Gao, X.N. Li, X.Y. Ren, Z.C. Kuang, Y.Q. Huang, T. Zhang, B. Liu, Elucidating the electrocatalytic CO_2 reduction reaction over a model single-atom nickel catalyst, Angew. Chem. Int. Ed. 59 (2020) 798–803.
[22] D.D. Wang, Z.X. Yuan, X.L. Wu, W. Xiong, J.Q. Ding, Z.H. Zhang, W.X. Huang, Ni single atoms confined in nitrogen-doped carbon nanotubes for active and selective hydrogenation of CO_2 to CO, ACS Catal. 13 (2023) 7132–7138.
[23] X.Y. Gong, D.C. Li, Q. Zhang, W.Q. Wang, Z.B. Tian, G. Su, M.H. Huang, G. H. Wang, Cobalt single atoms supported on monolithic carbon with a hollow-on-hollow architecture for efficient transfer hydrogenations, Nano Res. 16 (2023) 11358–11365.
[24] Y.P. Song, R. Guo, B.B. Feng, Y.H. Fu, F.M. Zhang, Y.F. Zhang, D.L. Chen, J. W. Zhang, W.D. Zhu, Coordination number engineering of Zn single-atom sites for enhanced transfer hydrogenation performance, Chem. Eng. J. 465 (2023), 142920.
[25] B.B. Feng, R. Guo, Q.L. Cai, Y.P. Song, N. Li, Y. Fu, D.L. Chen, J.W. Zhang, W. D. Zhu, F.M. Zhang, Construction of isolated Ni sites on nitrogen-doped hollow carbon spheres with $Ni–N_3$ configuration for enhanced reduction of nitroarenes, Nano Res. 15 (2022) 6001–6009.
[26] Q.L. Cai, Q.H. Xu, Y.Y. Zhang, Y.H. Fu, D.L. Chen, J.W. Zhang, W.D. Zhu, F. M. Zhang, Boosted catalytic hydrogenation performance using isolated Co sites anchored on nitrogen-incorporated hollow porous carbon, J. Phys. Chem. C 125 (2021) 5088–5098.
[27] T. Yang, X.N. Mao, Y. Zhang, X.P. Wu, L. Wang, M.Y. Chu, C.W. Pao, S.Z. Yang, Y. Xu, X.Q. Huang, Coordination tailoring of Cu single sites on C_3N_4 realizes selective CO_2 hydrogenation at low temperature, Nat. Commun. 12 (2021) 6022.
[28] J. Ding, Z.Y. Teng, X.Z. Su, K. Kato, Y.H. Liu, T. Xiao, W. Liu, L.Y. Liu, Q. Zhang, X. Y. Ren, J.C. Zhang, Z.Y. Chen, O. Teruhisa, A. Yamakata, H.B. Yang, Y.Q. Huang, B. Liu, Y.M. Zhai, Asymmetrically coordinated cobalt single atom on carbon nitride for highly selective photocatalytic oxidation of CH_4 to CH_3OH, Chem 9 (2023) 1017–1035.
[29] L. Wang, B.F. Ji, Y.P. Zheng, Y.B. Tang, Asymmetric coordination of Iridium single-atom IrN_3O boosting formic acid oxidation catalysis, Angew. Chem. Int. Ed. 62 (2023) e202301711.
[30] F.S. Yu, J.Y. Zhan, D.T. Chen, J.Y. Guo, S.B. Zhang, L.H. Zhang, Electronic states regulation induced by the synergistic effect of Cu clusters and $Cu-S_1N_3$ sites boosting electrocatalytic performance, Adv. Funct. Mater. 33 (2023) 2214425.
[31] K. Yuan, D. Lützenkirchen-Hecht, L.B. Li, L. Shuai, Y.Z. Li, R. Cao, M. Qiu, X. D. Zhuang, M.K.H. Leung, Y.W. Chen, U. Scherf, Boosting oxygen reduction of single iron active sites via geometric and electronic engineering: Nitrogen and phosphorus dual coordination, J. Am. Chem. Soc. 142 (2020) 2404–2412.
[32] J. Liu, S.Z. Qiao, H. Liu, J. Chen, A. Orpe, D.Y. Zhao, G.Q. Lu, Extension of the Stöber method to the preparation of monodisperse resorcinol–formaldehyde resin polymer and carbon spheres, Angew. Chem. Int. Ed. 50 (2011) 5947–5951.
[33] S.Y. Chen, T. Luo, X.Q. Li, K.J. Chen, J.W. Fu, K. Liu, C. Cai, Q.Y. Wang, H.M. Li, Y. Chen, C. Ma, L. Zhu, Y.R. Lu, T.S. Chan, M.S. Zhu, E. Cortés, M. Liu, Identification of the highly active $Co–N_4$ coordination motif for selective oxygen reduction to hydrogen peroxide, J. Am. Chem. Soc. 144 (2022) 14505–14516.
[34] G. Kresse, J. Furthmüller, Efficiency of ab-initio total energy calculations for metals and semiconductors using a plane-wave basis set, Comput. Mater. Sci. 6 (1996) 15–50.
[35] P.E. Blöchl, Projector augmented-wave method, Phys. Rev. B 50 (1994) 17953–17979.
[36] J.P. Perdew, J.A. Chevary, S.H. Vosko, K.A. Jackson, M.R. Pederson, D.J. Singh, C. Fiolhais, Atoms, molecules, solids, and surfaces: Applications of the generalized gradient approximation for exchange and correlation, Phys. Rev. B 46 (1992) 6671–6687.
[37] H.F. Wang, Z.P. Liu, Comprehensive mechanism and structure-sensitivity of ethanol oxidation on platinum: New transition-state searching method for resolving the complex reaction network, J. Am. Chem. Soc. 130 (2008) 10996–11004.

[38] C.X. Guo, X. Tian, X.Y. Fu, G.Q. Qin, J. Long, H. Li, H.J. Jing, Y.H. Zhou, J.P. Xiao, Computational design of spinel oxides through coverage-dependent screening on the reaction phase diagram, ACS Catal. 12 (2022) 6781–6793.
[39] C. Pan, F. Wu, J.J. Mao, W.J. Wu, G. Zhao, W.L. Ji, W.J. Ma, P. Yu, L.Q. Mao, Highly stable and selective sensing of hydrogen sulfide in living mouse brain with NiN_4 single-atom catalyst-based galvanic redox potentiometry, J. Am. Chem. Soc. 144 (2022) 14678–14686.
[40] S. Han, R.J. Gao, M.S. Sun, Y. Zhou, W.T. Chen, X.X. Liu, J.Z. Qin, D.J. Tao, Z. H. Zhang, Synergistic roles of single Co atoms and Co nanoparticles for the hydrodeoxygenation and ring hydrogenation reactions, J. Phys. Chem. C 127 (2023) 14185–14196.
[41] J.J. Shi, Y. Wei, D. Zhou, L.L. Zhang, X.F. Yang, Z.L. Miao, H.F. Qi, S.X. Zhang, A. Q. Li, X.Y. Liu, W.S. Yan, Z. Jiang, A.Q. Wang, T. Zhang, Introducing Co–O moiety to Co–N–C single-atom catalyst for ethylbenzene dehydrogenation, ACS Catal. 12 (2022) 7760–7772.
[42] X.X. Liu, J.Z. Qin, W. Dai, Z.H. Zhu, P. Zhou, Y.X. Wang, J.B. Nie, Y.K. Yang, Z. H. Zhang, Metal-free and additive-free synthesis of imides and nitriles from ketones via oxidative cleavage of C(O)–C bonds, ACS Catal. 12 (2022) 13300–13311.
[43] C. Tang, L. Chen, H.J. Li, L.Q. Li, Y. Jiao, Y. Zheng, H.L. Xu, K. Davey, S.Z. Qiao, Tailoring acidic oxygen reduction selectivity on single-atom catalysts via modification of first and second coordination spheres, J. Am. Chem. Soc. 143 (2021) 7819–7827.
[44] H.H. Luo, L.Y. Wang, S.S. Shang, G.S. Li, Y. Lv, S. Gao, W. Dai, Cobalt nanoparticles-catalyzed widely applicable successive C—C bond cleavage in alcohols to access esters, Angew. Chem. Int. Ed. 59 (2020) 19268–19274.
[45] L.V.A. Hale, N.K. Szymczak, Hydrogen transfer catalysis beyond the primary coordination sphere, ACS Catal. 8 (2018) 6446–6461.
[46] M.H. Li, S.Y. Chen, Q.K. Jiang, Q.L. Chen, X. Wang, Y. Yan, J. Liu, C.C. Lv, W. P. Ding, X.F. Guo, Origin of the activity of Co–N–C catalysts for chemoselective hydrogenation of nitroarenes, ACS Catal. 11 (2021) 3026–3039.
[47] W.H. Wang, J.T. Muckerman, E. Fujita, Y. Himeda, Mechanistic insight through factors controlling effective hydrogenation of CO2 catalyzed by bioinspired proton-responsive iridium(III) complexes, ACS Catal. 3 (2013) 856–860.
[48] H. Lv, H.Y. Qin, K. Ariga, Y. Yamauchi, B. Liu, A general concurrent template strategy for ordered mesoporous intermetallic nanoparticles with controllable catalytic performance, Angew. Chem. Int. Ed. 61 (2022) e202116179.